was carried out, the bisoxazolidine **24** formed was unsymmetrical, with one of the oxazolidine rings epimeric with the other. The pseudo-S_2 symmetry of **24** forces the two oxazolidine centres (marked with asterisks in Fig. 7) to seek pseudo-enantiomeric conformations, which can only happen if one oxazolidine adopts unusual *endo* relative stereochemistry[28], allowing it to retain the favourable oxazolidine–amide interaction.

Extending information transmission in these systems beyond the 2.5 nm reported here will depend on the efficacy of additional coupling reactions: the conformational relay itself seems remarkably robust, with no significant degradation of information quality even after six relay steps. The synthetic versatility of amides, and in particular their ability to act as branch points, may make related compounds valuable components of future molecular devices for the transmission and processing of information[15,16]. □

Received 26 May; accepted 10 August 2004; doi:10.1038/nature02933.

1. Krauss, G. *Biochemistry of Signal Transduction and Regulation* (Wiley-VCH, Weinheim, 1999).
2. Perutz, M. *Mechanisms of Cooperativity and Allosteric Regulation in Proteins* (Cambridge Univ. Press, Cambridge, 1990).
3. Eliel, E. L. & Wilen, S. H. *Stereochemistry of Organic Compounds* Ch. 12 (Wiley, New York, 1994).
4. Mikami, K., Shimizu, M., Zhang, H.-C. & Maryanoff, B. E. Acyclic stereocontrol between remote atom centers via intramolecular and intermolecular stereo-communication. *Tetrahedron* **57,** 2917–2951 (2001).
5. Linnane, P., Magnus, N. & Magnus, P. Induction of molecular asymmetry by a remote chiral group. *Nature* **385,** 799–801 (1997).
6. Clayden, J., Mitjans, D. & Youssef, L. H. Lithium-sulfoxide-lithium exchange for the asymmetric synthesis of atropisomers under thermodynamic control. *J. Am. Chem. Soc.* **124,** 5266–5267 (2002).
7. Clayden, J. & Lai, L. W. (−)-Ephedrine as an auxiliary for the asymmetric synthesis of atropisomeric amides by dynamic resolution under thermodynamic control. *Tetrahedron Lett.* **42,** 3163–3166 (2001).
8. Clayden, J., Lai, L. W. & Helliwell, M. Using amide conformation to "project" the stereochemistry of a (−)-ephedrine-derived oxazolidine: a pair of pseudoenantiomeric chiral amido-phosphine ligands. *Tetrahedron* **12,** 695–698 (2001).
9. Clayden, J. & Lai, L. W. Enantioselective synthesis of atropisomeric amides by dynamic resolution: thermodynamic control with a proline-derived diamine resolving agent. *Angew. Chem. Intl Edn* **38,** 2556–2558 (1999).
10. Clayden, J., Pink, J. H. & Yasin, S. A. Conformationally interlocked amides: remote asymmetric induction by mechanical transfer of stereochemical information. *Tetrahedron Lett.* **39,** 105–108 (1998).
11. Clayden, J., Kenworthy, M. N. & Youssef, L. H. Axial chirality in xanthene-4,5-dicarboxamides: 1,9-stereocontrol mediated by remote interactions between conformationally constrained amide groups. *Tetrahedron Lett.* **41,** 5171–5174 (2000).
12. Clayden, J., Lund, A. & Youssef, L. H. Conformational preference and remote (1,10) stereocontrol in biphenyl-2,2′-dicarboxamides. *Org. Lett.* **3,** 4133–4136 (2001).
13. Clayden, J. Stereocontrol with rotationally restricted amides. *Synlett*, 810–816 (1998).
14. Krauss, R. & Koert, U. Molecular signal transduction by conformational transmission. *Synlett*, 598–608 (2003).
15. Balzani, V., Credi, A. & Venturi, M. The bottom-up approach to molecular-level devices and machines. *Chem. Eur. J.* **8,** 5524–5542 (2002).
16. Sauvage, J.-P. Transition-metal containing rotaxanes and catenanes in motion: toward molecular machines and motors. *Acc. Chem. Res.* **31,** 611–619 (1998).
17. Cuyegkeng, M. A. & Mannschreck, A. Chromatographic separation of enantiomers and barriers to enantiomerization of axially chiral aromatic carboxamides. *Chem. Ber.* **120,** 803–809 (1987).
18. Bowles, P. *et al.* Atroposelectivity in the reactions of ortholithiated tertiary amides with aldehydes. *J. Chem. Soc. Perkin Trans.* **1,** 2607–2616 (1997).
19. Ahmed, A. *et al.* Barriers to rotation about the chiral axis of tertiary aromatic amides. *Tetrahedron* **54,** 13277–13294 (1998).
20. Snieckus, V. Directed ortho metalation. Tertiary amide and O-carbamate directors in synthetic strategies for polysubstituted aromatics. *Chem. Rev.* **90,** 879–933 (1990).
21. Yin, J., Rainka, M. P., Zhang, X.-X. & Buchwald, S. L. A highly active Suzuki catalyst for the synthesis of sterically hindered biaryls: novel ligand coordination. *J. Am. Chem. Soc.* **124,** 1162–1163 (2002).
22. Clayden, J., Lai, L. W. & Helliwell, M. Dynamic resolution of atropisomeric amides using proline-derived imidazolidines and ephedrine-derived oxazolidines. *Tetrahedron* **60,** 4399–4412 (2004).
23. Clayden, J., McCarthy, C., Westlund, N. & Frampton, C. S. Atroposelective attack of nucleophiles on 2-formyl-1-naphthamides and their derivatives: chelation and non-chelation control. *J. Chem. Soc. Perkin Trans.* **1,** 1363–1378 (2000).
24. Date, M. *et al.* Efficient 1,8- and 1,9-asymmetric inductions in the Grignard reaction of δ- and ε-keto esters of 1,1′-binaphthalen-2-ols with an oligoether tether as the 2′-substituent: application to the synthesis of (-)-malyngolide. *J. Chem. Soc. Perkin Trans.* **1,** 645–653 (2001).
25. Tamai, Y. *et al.* Efficient 1,8- to 1,12-asymmetric induction in Grignard reactions of ω-keto esters by using BINOL or its 2′-oligoether derivatives as the chiral auxiliary. *J. Chem. Soc. Perkin Trans.* **1,** 1141–1142 (1999).
26. Magnus, N. & Magnus, P. 1,13- and 1,14-asymmetric induction; remote control. *Tetrahedron Lett.* **38,** 3491–3494 (1997).
27. Heinemann, C. & Demuth, M. Short biomimetic synthesis of a steroid by photoinduced electron transfer and remote asymmetric induction. *J. Am. Chem. Soc.* **121,** 4894–4895 (1999).
28. Agami, C. & Rizk, T. Kinetic control of asymmetric induction during oxazolidine formation from (−)-ephedrine and aromatic aldehydes. *Tetrahedron* **41,** 537–540 (1985).

Supplementary Information accompanies the paper on **www.nature.com/nature**.

Acknowledgements We are grateful to the EPSRC for support of this work.

Competing interests statement The authors declare that they have no competing financial interests.

Correspondence and requests for material should be addressed to J. C. (clayden@man.ac.uk). The Cambridge Crystallographic Database deposition numbers for X-ray crystal structures are, for **9**, 244658 and for **20**, 244659.

Extreme climate of the global troposphere and stratosphere in 1940–42 related to El Niño

S. Brönnimann[1,2], J. Luterbacher[3], J. Staehelin[1], T. M. Svendby[4], G. Hansen[5] & T. Svenøe[6]

[1]*Institute for Atmospheric and Climate Science, ETH Zürich, Hönggerberg HPP, CH-8093 Zürich, Switzerland*
[2]*Lunar and Planetary Laboratory, University of Arizona, Tucson, Arizona 85721, USA*
[3]*NCCR Climate and Institute of Geography, University of Bern, Hallerstrasse 12, CH-3012 Bern, Switzerland*
[4]*Department of Physics, University of Oslo, PO Box 1048, Blindern, N-0316 Oslo, Norway*
[5]*Norwegian Institute for Air Research, Polar Environmental Centre, Hjalmar Johansens Gate 14, N-9296 Tromsø, Norway*
[6]*Norwegian Polar Institute, Ny-Ålesund, PO Box 505, N-9171 Longyearbyen, Norway*

Although the El Niño/Southern Oscillation phenomenon is the most prominent mode of climate variability[1] and affects weather and climate in large parts of the world, its effects on Europe and the high-latitude stratosphere are controversial[2–5]. Using historical observations and reconstruction techniques, we analyse the anomalous state of the troposphere and stratosphere in the Northern Hemisphere from 1940 to 1942 that occurred during a strong and long-lasting El Niño event. Exceptionally low surface temperatures in Europe and the north Pacific Ocean coincided with high temperatures in Alaska. In the lower stratosphere, our reconstructions show high temperatures over northern Eurasia and the north Pacific Ocean, and a weak polar vortex. In addition, there is observational evidence for frequent stratospheric warmings and high column ozone at Arctic and mid-latitude sites. We compare our historical data for the period 1940–42 with more recent data and a 650-year climate model simulation. We conclude that the observed anomalies constitute a recurring extreme state of the global troposphere–stratosphere system in northern winter that is related to strong El Niño events.

Scientists in the early 1940s observed unusually high values of total ozone over several sites in Europe, but did not present an explanation. At the same time, exceptional climatic conditions were registered at the Earth's surface, but were never analysed in a large-scale context. Moreover, a prolonged El Niño occurred in 1939–42, raising the question of a possible relation between El Niño, European climate, and the northern stratosphere[6]. In order to study this period in detail, we have compiled, digitized and re-evaluated all available total ozone observations[7–9] and several tens of thousands of geopotential height (GPH) and temperature profiles from radio-

sondes and aircraft from 1939–44[10]. The latter served to statistically reconstruct monthly mean fields of GPH and temperature for the northern extratropics up to the 100 hPa level in the lower stratosphere (around 16 km altitude)[11]. Here we analyse these data and compare the results to more recent data and a climate model simulation.

The El Niño event started in autumn 1939, reached full strength in January 1940 and lasted, with varying intensity, until spring 1942 (Supplementary Fig. 1). The characteristic anomalies in the northern extratropics described below began in December 1939 or January 1940 and ended between February and April 1942, with a considerable persistence during this period (Supplementary Fig. 1). In the following we focus on the extended winter period (January to April; the season most indicative of large-scale coupling processes) of the years 1940, 1941 and 1942. Averaged anomaly fields are shown in Fig. 1 (top). In order to assess the magnitude of the individual anomaly features, corresponding time series for the twentieth century are shown in Fig. 2, together with the El Niño index NINO3.4, the Pacific Decadal Oscillation index (PDOI) and the North Atlantic Oscillation index (NAOI; for definitions, see Methods).

The dominant global feature was the contrast between high tropical and low extratropical sea surface temperatures (SSTs) in both hemispheres, most pronounced in the Pacific (reflected by exceptional peaks in NINO3.4 and PDOI). Surface air temperatures (SATs) were exceptionally high in Alaska, Canada and central Asia (Fig. 1), but low in Siberia and extremely low in central and northeastern Europe, where the three severe winters in a row (T_{Euro} in Fig. 2) played an important role in the Second World War. A similar, large-scale temperature pattern also appeared in summer and autumn 1940 and 1941, though weaker in magnitude (Supplementary Fig. 2). The dominant features in the wintertime sea level pressure field (SLP, Fig. 1) were a weak Icelandic low and an intensified Aleutian low; their anomaly difference (IL–AL in Fig. 2) was twice as large in 1940 and 1941 than at any other time in the twentieth century. The weak Icelandic low and Azores high led to a strongly negative NAOI. Positive SLP deviations were observed over Scandinavia and North America, and negative deviations over Labrador and Manchuria. Distinct anomaly patterns are also found in the reconstructed upper-level fields (see Methods). The 300 hPa GPH field reflects an anomaly in planetary wave structure; positive deviations appear over Canada and Greenland, negative deviations over the western North Pacific, parts of the North Atlantic, and central Europe. At the Earth's surface and in the troposphere, the period 1940–42 represents an extreme climatic anomaly of hemispheric to global extent.

Re-evaluated upper-air data and reconstructions[11] reveal that this is also the case in the stratosphere. The wintertime 100 hPa GPH anomaly field (Fig. 1 top) shows a large difference between the polar region and the mid-latitudes (Z100 in Fig. 2), indicating a weak and meridionally expanded polar vortex. Temperatures at 100 hPa exhibit a positive anomaly over northern Eurasia and the North Pacific, and negative anomalies over the northern Atlantic and Canada. The data suggest a frequent occurrence of major midwinter stratospheric warmings (MMW, at least in January 1940, February 1941 and February 1942)[12]. The anomaly in stratospheric circulation was accompanied by large total ozone deviations. A strong positive anomaly around 1940–42 appears in all six available ozone series (Fig. 3), at sites spread throughout the Northern Hemisphere. The same is found for lower-quality series from Oxford, UK[13], and Table Mountain, California[14]. The highest annual mean values in the series from Arosa in Switzerland (since 1926) and Tromsø in the Norwegian Arctic (since 1935) both occurred in 1940 (Fig. 2; note that anthropogenic ozone depletion affects total ozone after around 1970). Chemical effects can largely be excluded—rather, the total ozone data point to an extreme perturbation of ozone transport, and hence circulation, in the stratosphere.

Analysed in context of twentieth-century climate variability, the 1940–42 period stands out as an anomaly unique in strength, but weaker anomalies of the same type are also found after 1948. There

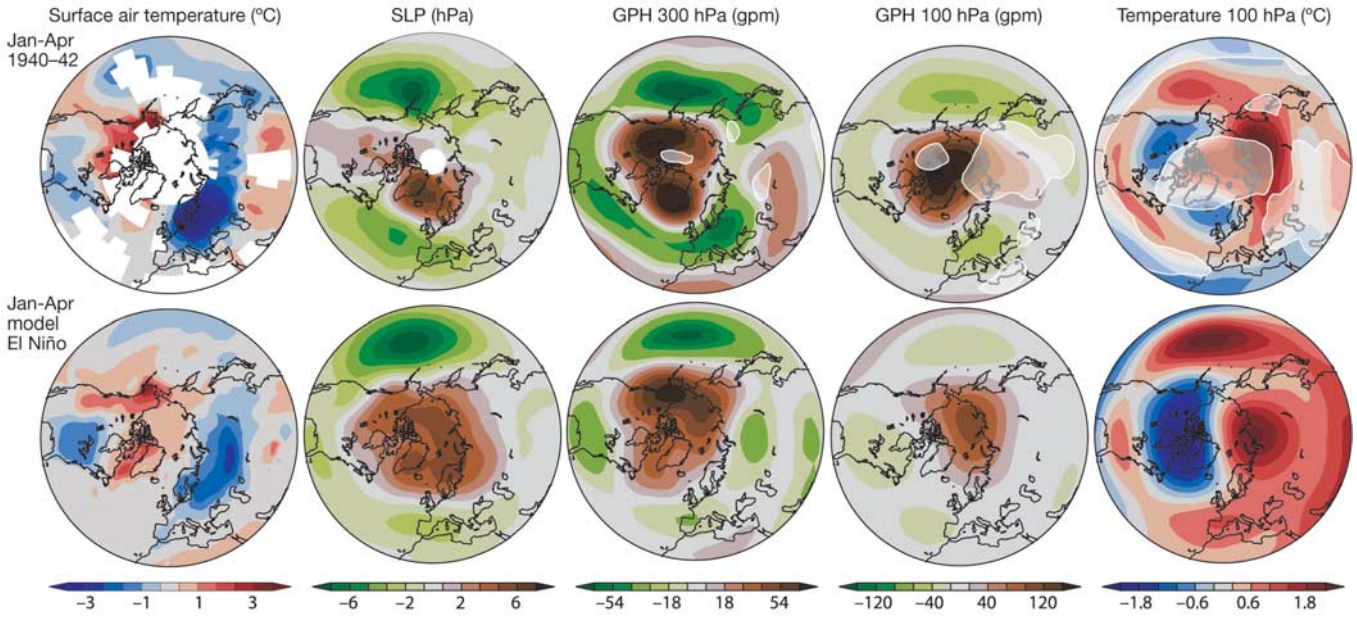

Figure 1 Consistent northern winter climate extremes related to strong El Niño events. Top, polar stereographic projection of anomaly fields (with respect to 1961–90) of surface air temperature[27], sea level pressure (SLP)[29], 300 hPa and 100 hPa geopotential height (GPH in units of geopotential metres, gpm) and 100 hPa temperature[11], in the northern extratropics averaged from January to April, 1940–42. Light shadings denote a low reconstruction skill (reduction of error RE <0.2 based on two split sample validations[11]). Bottom, same anomaly fields for the winters during the 26 strongest El Niño years (October–September NINO3.4 >1 °C) in the CCSM-2.0 control run.

are seven cases where all index series relating to the Atlantic-European sector and the stratosphere (NAOI, T_{Euro}, Z100, total ozone at Arosa and Tromsø), after removing an 11-yr moving average to account for trends and possible solar cycle effects, have the same sign as in 1940–42. All of these cases—the most pronounced were 1969/70, 1987 and 1998—concur with El Niño conditions (positive NINO3.4), which therefore are considered as a possible driving factor.

The anomalies in the Pacific region can at least partly be attributed to El Niño, which is known to affect the North Pacific and surrounding areas via changes in the Hadley circulation and Rossby wave generation[15,16]. Possible low-frequency oceanic processes and ocean–atmosphere feedbacks in the North Pacific might also have contributed to the cold central North Pacific and strong Aleutian low in 1940/41 and 1987[17,18]. As to the Atlantic-European sector, the anomalies at the surface and in the stratosphere are dynamically consistent with each other. The wintertime relation between the Icelandic low and the polar vortex and their effect on European climate and total ozone are well documented[19–21]. To what extent European winter climate and the northern stratosphere are affected by El Niño is a matter of debate[2–5]. According to several observational and modelling studies, the 'canonical' El Niño winter signal in Europe consists of cold temperatures in Northern Europe, high SLP from Iceland to Scandinavia and low SLP over central and western Europe[2,4,22], as in 1940–42. Also, strong El Niños have been found to be associated with a weak polar vortex and more frequent major stratospheric warmings[5,6]. However, not all El Niños show these features and other studies find no consistent signal, which may be due to the strong variability of extratropical circulation, the small number of strong events, disturbing effects of volcanic eruptions and anthropogenic influences, interference with the Quasi Biennial Oscillation in the stratosphere[5,6], or a varying, non-stationary signal[4,16]. In summary, all anomalies found in 1940–42 are qualitatively consistent with El Niño influence.

To further explore the concurrence of extremes in Pacific and European climate and the northern stratosphere and their possible relation to El Niño, we used a 650-yr control run of a coupled climate model (CCSM-2.0) and calculated the same index series as in Fig. 2. Extremes in the different series tend to be concomitant. Selecting only strong El Niño years (October–September average of NINO3.4 >1 °C, 26 cases in 650 yr), significant deviations of the same sign as in 1940–42 appear in all series (Fig. 2 right, the selected year is denoted 0). The mean wintertime anomaly fields for these cases (Fig. 1 bottom) show a strong similarity to those of the early 1940s, not only with respect to SAT and SLP, but also the planetary wave structure and strength of the polar vortex, as evident in 300 and 100 hPa GPH. Even for 100 hPa temperature we find the same characteristic pattern. In addition, the selected El Niño years exhibit very similar SAT patterns as in 1940 and 1941 for summer and, to a lesser extent, autumn (Supplementary Fig. 2). These results confirm that, first, the concurrence of the characteristic anomalies in 1940–42 represents a consistent extreme state of the global troposphere–stratosphere system on interannual timescales. Second, they suggest that this extreme state can be related to strong El Niños.

The CCSM-2.0 model does not simulate stratospheric ozone. Nevertheless, analysing further dynamical properties can give important indications with respect to stratosphere–troposphere coupling and stratospheric ozone. We find a significant increase

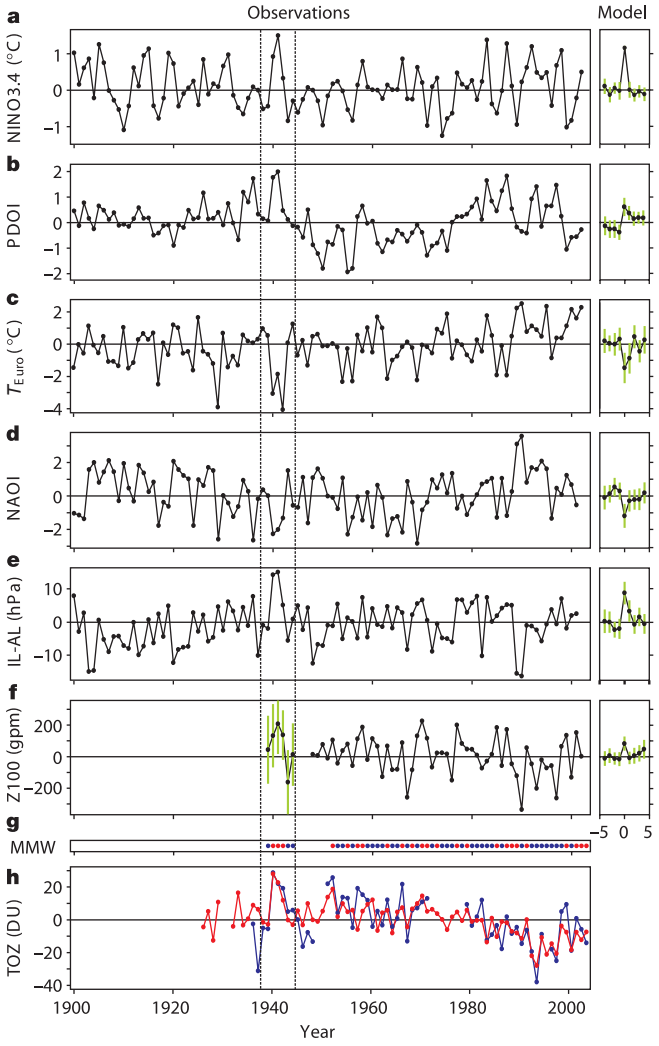

Figure 2 Climate indices and total ozone series from 1900 to 2003 (left) and composite series for the 26 strongest El Niño years (preceding and following 4 yr are also shown) in the CCSM-2.0 control run (right). **a**, NINO3.4 (ref. 26); **b**, PDOI (ref. 28); **c**, T_{Euro}; **d**, NAOI; **e**, IL-AL; **f**, Z100; **g**, occurrence (red) or absence (blue) of major midwinter (December–February) stratospheric warmings (MMW)[12,31]; and **h**, total ozone at Arosa[7] (red) and Tromsø (blue). **a**, **b** and **h** are annual averages, **c**–**f** are January–April averages (see Methods). Green bars give 95% confidence intervals for reconstructions (left, **f**) and mean values (right, **a**–**f**). Dashed lines denote the 1938–44 period.

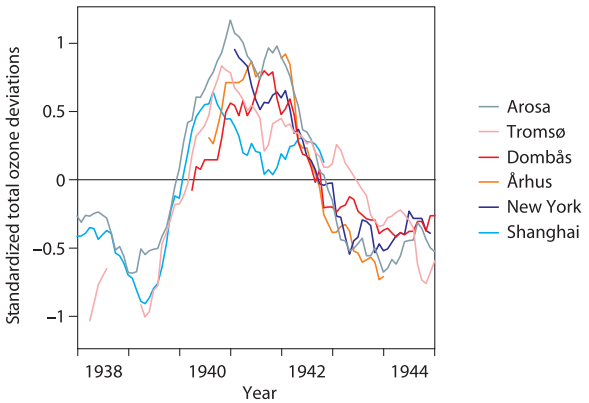

Figure 3 The 1940–42 total ozone anomaly. Standardized monthly anomalies (with respect to the 1938–44 mean annual cycle) of total ozone at Arosa (Switzerland)[7], Tromsø, Dombås[8] (both Norway), Århus (Denmark)[9], New York (USA)[9] and Shanghai (China)[9] smoothed with a 12-month moving average.

in the zonally averaged, early-to-midwinter (November–February) meridional eddy heat flux at 100 hPa (45°–75° N) in the selected El Niño years, suggesting that more upward propagating planetary wave activity reached the stratosphere. A stronger wave activity flux diminishes the strength of the polar vortex and strengthens the meridional circulation in the middle stratosphere[23,24]. It leads to more ozone transport from the tropical source regions to the extratropics[24], stronger descent over the polar area and hence a warm lower stratosphere[23] and high Arctic total ozone in late winter[24]. Furthermore, pulses of increased upward propagating wave activity act as trigger for major stratospheric warmings[25]. Hence, this mechanism is qualitatively consistent with all stratospheric features of the 1940–42 anomaly (for which no heat flux can be calculated). It not only provides an explanation for the total ozone increase in the Arctic but would also contribute, together with ozone redistribution in the lower stratosphere owing to the change in planetary wave structure[12], to the total ozone increase at mid-latitudes.

The results suggest that the global climate anomaly in 1940 to 1942—previously poorly documented—constitutes a key period for our understanding of large-scale climate variability and global El Niño effects. □

Methods

Climate model

CCSM-2.0 is a coupled, global climate model with four components (ocean, atmosphere, land, sea ice). We used the control run b20.007 provided by the University Corporation for Atmospheric Research, Boulder, Colorado (for documentation see http://www.ccsm.ucar.edu/models/ccsm2.0/). The model was run fully coupled for 370 yr in a spin-up mode with constant 1990 conditions. The final control run was continued from year 350 and was run fully coupled until year 999. The atmospheric component CAM1 was run in a T42 horizontal spectral resolution with 26 levels. Ozone concentrations were fixed to the 1990 annual cycle. Note that this includes ozone-hole conditions over Antarctica, not representative of 1940–42 conditions. However, we expect no strong effect on the circulation of the northern extratropics. We used monthly averages for the years 350–999.

Climate indices

Several climate indices were calculated based on monthly mean values. NINO3.4 (ref. 26), T_{NPac}, T_{Alaska} and T_{Euro} are averaged temperature anomalies for the areas 5° S–5° N/120°–170° W, 30°–50° N/155°–225° E, 50°–75° N/180°–240° E and 45°–70° N/20°–55° E, respectively (HadCRUT2v data, consisting of SAT over land areas merged with SST[27]). The PDOI is the amplitude, defined for all calendar months, of the first principal component of monthly North Pacific SSTs (poleward of 20° N) obtained from October to March[28]. Z100 is the difference in 100 hPa GPH anomalies between 75°–90° N and 40°–55° N, IL and AL are SLP[29] anomalies for the areas 60°–70° N/10°–40° W and 40°–55° N/140°–170° W, respectively. The NAOI is the difference of standardized SLP[29] anomalies at 64.13° N/21.9° W and 37.73° N/23.7° W. In order to obtain annual series, T_{Euro}, Z100, NAOI and IL-AL were averaged from January to April, when large-scale coupling processes are expected to be most influential[20,23,24]. Annual averages were used for PDOI, total ozone (calendar year) and NINO3.4 (October of previous year to September, thus leading all extratropical indices by three months), because anomalies in total ozone and SST have a long persistence. Monthly meridional (transient plus stationary) eddy heat flux was calculated from the model data as $\langle v' T' \rangle + \langle v \rangle^{*} \langle T \rangle^{*}$, where v and T denote instantaneous meridional wind and temperature, respectively, $\langle\,\rangle$ denotes a monthly average, and primes and stars denote deviations from monthly and zonal averages, respectively. It was subsequently zonally averaged between 45° and 75° N from November to February. The chosen lead of two months with respect to Z100 maximizes the correlation with Z100 ($r = 0.75$), consistent with other studies[23]. Upper-level fields were reconstructed from historical radiosonde and aircraft data as well as SAT station data and SLP by means of principal component regression models calibrated in the 1948–94 period[11]. They were supplemented with NCEP/NCAR reanalysis[30] after 1948. Unless otherwise noted, anomalies refer to the 1961–90 mean annual cycle (years 350–999 in the CCSM-2.0 data). For the determination of spatial or temporal averages, 50% of the data must be available. Spatial averages from gridded data were obtained using the grid cell areas as weights. Tests and 95% confidence intervals for mean values were calculated assuming a t-distribution.

Total ozone

The Tromsø total ozone data 1935–49 were homogenized partially by introducing empirical correction factors. The measurements before 15 August 1939 performed with an older instrument (Fery spectrograph) were homogenized with the later measurements (Dobson spectrophotometer) based on simultaneous measurements in the period August 1939 to September 1940 (scaling factor of 1.37). Zenith sky measurements 1940–49 were adjusted by calculating ratios of pure direct-sun/zenith-blue daily means and daily means including zenith-cloud measurements, yielding consistent correction factors (T.S. and G.H., manuscript in preparation). After November 1978, the record was supplemented with TOMS Version 7 overpass data in order to fill gaps. For all series, monthly means were calculated if at least six daily values were available in order to include winter months with sparse data (most monthly means are based on more than 15 values).

Received 16 April; accepted 27 August 2004; doi:10.1038/nature02982.

1. Diaz, H. & Markgraf, V. (eds) *El Niño and the Southern Oscillation: Multiscale Variability and Global and Regional Impacts* (Cambridge Univ. Press, Cambridge, UK, 2000).
2. Fraedrich, K. & Müller, K. Climate anomalies in Europe associated with ENSO extremes. *Int. J. Climatol.* **12,** 25–31 (1992).
3. Pozo-Vázquez, D., Esteban-Parra, M. J., Rodrigo, F. S. & Castro-Diez, Y. The association between ENSO and winter atmospheric circulation and temperature in the North Atlantic region. *J. Clim.* **14,** 3408–3420 (2001).
4. Graetbatch, R. J., Lu, J. & Peterson, K. A. Nonstationary impact of ENSO on Euro-Atlantic winter climate. *Geophys. Res. Lett.* **31,** doi:10.1029/2003GL018542 (2004).
5. van Loon, H. & Labitzke, K. The Southern Oscillation. Part V: The anomalies in the lower stratosphere of the Northern Hemisphere in winter and a comparison with the Quasi-Biennial Oscillation. *Mon. Weath. Rev.* **115,** 357–369 (1987).
6. Labitzke, K. G. & van Loon, H. *The Stratosphere. Phenomena, History, and Relevance* (Springer, Berlin, 1999).
7. Staehelin, J. *et al.* Total ozone series of Arosa (Switzerland). Homogenization and data comparison. *J. Geophys. Res.* **103,** 5827–5841 (1998).
8. Svendby, T. M. Reanalysis of total ozone measurements at Dombås and Oslo, Norway, from 1940 to 1949. *J. Geophys. Res.* **108,** doi:10.1029/2003JD003963 (2003).
9. Brönnimann, S., Cain, J. C., Staehelin, J. & Farmer, S. F. G. Total ozone observations prior to the IGY. II: Data and quality. *Q. J. R. Meteorol. Soc.* **129,** 2819–2843 (2003).
10. Brönnimann, S. A historical upper-air data set for the 1939–1944 period. *Int. J. Climatol.* **23,** 769–791 (2003).
11. Brönnimann, S. & Luterbacher, J. Reconstructing Northern Hemisphere upper-level fields during World War II. *Clim. Dyn.* **22,** 499–510 (2004).
12. Brönnimann, S., Luterbacher, J., Staehelin, J. & Svendby, T. M. An extreme anomaly in stratospheric ozone over Europe in 1940–1942. *Geophys. Res. Lett.* **31,** doi: 10.1029/2004GL019611 (2004).
13. Goldsmith, P., Tuck, A. F., Foot, J. S., Simmons, E. L. & Newson, R. L. Nitrogen oxides, nuclear weapon testing, Concorde and stratospheric ozone. *Nature* **244,** 545–551 (1973).
14. Angione, R. J. & Roosen, R. G. Baseline ozone results from 1923 to 1955. *J. Clim. Appl. Meteorol.* **22,** 1377–1383 (1983).
15. Alexander, M. A. *et al.* The atmospheric bridge: Influence of ENSO teleconnnections on air-sea interaction over the global oceans. *J. Clim.* **15,** 2205–2231 (2002).
16. Trenberth, K. E. *et al.* Progress during TOGA in understanding and modeling global teleconnections associated with tropical sea surface temperatures. *J. Geophys. Res.* **103,** 14291–14324 (1998).
17. Chavez, F. P., Ryan, J., Lluch-Cota, S. E. & Ñiquen C., M. From anchovies to sardines and back: Multidecadal change in the Pacific Ocean. *Science* **299,** 217–221 (2003).
18. Trenberth, K. E. & Hurrell, J. W. Decadal atmosphere-ocean variations in the Pacific. *Clim. Dyn.* **9,** 303–319 (1994).
19. Ambaum, M. H. P. & Hoskins, B. J. The NAO troposphere-stratosphere connection. *J. Clim.* **15,** 1969–1978 (2002).
20. Hurrell, J., Kushnir, Y., Ottersen, G. & Visbeck, M. (eds) *The North Atlantic Oscillation. Climatic Significance and Environmental Impact* (AGU, Washington DC, 2003).
21. Staehelin, J., Harris, N. R. P., Appenzeller, C. & Eberhard, J. Ozone trends: A review. *Rev. Geophys.* **39,** 231–290 (2001).
22. Merkel, U. & Latif, M. A high resolution AGCM study of the El Niño impact on the North Atlantic/European sector. *Geophys. Res. Lett.* **29,** doi:10.1029/2001GL013726 (2002).
23. Newman, P. A., Nash, E. R. & Rosenfield, J. What controls the temperature of the arctic stratosphere during the spring? *J. Geophys. Res.* **106,** 19999–20010 (2001).
24. Randel, W. J., Wu, F. & Stolarski, R. Changes in column ozone correlated with the stratospheric EP flux. *J. Meteorol. Soc. Jpn* **80,** 849–862 (2002).
25. Limpasuvan, V., Thompson, D. W. J. & Hartmann, D. L. The life cycle of the Northern Hemisphere stratospheric sudden warmings. *J. Clim.* **17,** 2584–2597 (2004).
26. Kaplan, A. *et al.* Analyses of global sea surface temperature 1856–1991. *J. Geophys. Res.* **103,** 18567–18589 (1998).
27. Jones, P. D. & Moberg, A. Hemispheric and large-scale surface air temperature variations: An extensive revision and update to 2001. *J. Clim.* **16,** 206–223 (2003).
28. Mantua, N. J., Hare, S. R., Zhang, Y., Wallace, J. M. & Francis, R. C. A Pacific decadal climate oscillation with impacts on salmon. *Bull. Am. Meteorol. Soc.* **78,** 1069–1079 (1997).
29. Trenberth, K. E. & Paolino, D. A. The Northern Hemisphere sea level pressure data set: Trends, errors, and discontinuities. *Mon. Weath. Rev.* **108,** 855–872 (1980).
30. Kistler, R. *et al.* The NCEP-NCAR 50-year reanalysis: Monthly means CD-ROM and documentation. *Bull. Am. Meteorol. Soc.* **82,** 247–268 (2001).
31. Labitzke, K. G. & Naujokat, B. The lower Arctic stratosphere in winter since 1952. *SPARC Newsl.* **15,** 11–14 (2000).

Supplementary Information accompanies the paper on **www.nature.com/nature**.

Acknowledgements S.B. was funded by the Swiss National Science Foundation, the Holderbank Foundation and the Janggen-Poehn Foundation. J.L. was funded by the Swiss National Science Foundation (NCCR climate). Surface temperature and NCEP/NCAR reanalysis data were provided by Climatic Research Unit, (Norwich, UK) and the NOAA-CIRES Climate Diagnostics Center (Boulder, USA), respectively. SLP and CCSM-2.0 data were provided by NCAR/UCAR (Boulder, USA). We thank P. Della-Marta for English corrections.

Competing interests statement The authors declare that they have no competing financial interests.

Correspondence and requests for materials should be addressed to S. B. (stefan.broennimann@env.ethz.ch).